Journal of Materials Chemistry C

Accepted Manuscript

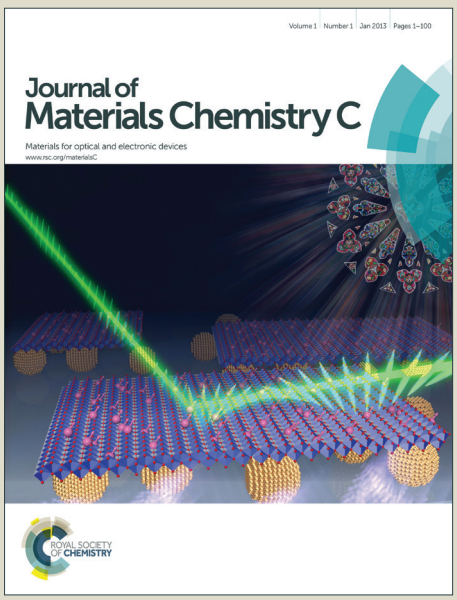

ROYAL SOCIETY OF CHEMISTRY

www.rsc.org/materialsC

Journal of
Materials Chemistry C RSC Publishing

ARTICLE

Photoluminescence properties of single-component white-emitting $Ca_9Bi(PO_4)_7$:Ce^{3+}, Tb^{3+}, Mn^{2+} phosphors for UV LEDs

Cite this: DOI: 10.1039/x0xx00000x

Received,
Accepted

DOI: 10.1039/x0xx00000x

www.rsc.org/

Kai Li,[ab] Mengmeng Shang,[a] Yang Zhang,[ab] Jian Fan,[a] Hongzhou Lian*[a] and Jun Lin*[a]

Co-doping Ce^{3+}/Eu^{2+}, Tb^{3+}, Mn^{2+} ions into a single-component host is commonly used to achieve white-light phosphors through energy transfer, which present good color stability and high color rendering index (CRI) value. In this work, a series of single-component trichromatic white-light-emitting $Ca_9Bi(PO_4)_7$(CBPO):Ce^{3+}, Tb^{3+}, Mn^{2+} phosphors were synthesized and investigated. The crystal structure, luminescence properties and the energy transfer behavior are discussed in detail. The energy transfer process from Ce^{3+} to Tb^{3+}/Mn^{2+} has been demonstrated to be a resonant type via the dipole–dipole/quadrupole-quadrupole interaction mechanism, respectively, which makes the emission color shift from purple-blue to green/red with the corresponding Commission Internationale deL'Eclairage (CIE) chromaticity coordinate from (0.166, 0.011) to (0.260, 0.569) and (0.582, 0.287), respectively. Additionally, the white emission by controlling the concentration ratio of Tb^{3+}, Mn^{2+} ions has been acquired in CBPO:0.08Ce^{3+}, 0.22Tb^{3+}, 0.11Mn^{2+} sample with the CIE chromaticity coordinate of (0.375, 0.310) and absolute quantum yield of 50% upon 292 nm excitation. The maximum quantum yield is 84% for CBPO:0.08Ce^{3+}, 0.90Tb^{3+}. The good thermal stability of CBPO:0.08Ce^{3+}, 0.22Tb^{3+},0.11Mn^{2+} sample shows about 83.6% at 150 °C of its initial PL intensity at room temperature, which attracts our more attention. The results suggest the present phosphors can be potentially applied as a candidate of single-component white-light phosphor for UV-pumped w-LED.

1. Introduction

Recently, a large amount of attention and increasing interest have been focused on white light-emitting diodes (w-LEDs) by virtue of their superior characters such as long operation lifetime, high luminous efficiency, low consumption of energy and ecofriendly constituents compared with conventional incandescent and fluorescent lamps.[1] Therefore, it is believed that w-LEDs will replace them completely as the fourth generation light source in the coming future. Typically, most commercial w-LEDs are produced via employing blue LED chips with yellow phosphors YAG:Ce^{3+} (YAG).[2] However, the deficiency of red component brings about the low color-rendering index (R_a) and high correlated color temperature (CCT), which would like to severely affect its quality for application. Accordingly, an alternative method, namely, using near ultraviolet n-UV or UV LEDs coupled with red, green, and blue phosphors, is developed to overcome above drawbacks.[3] However, there exists the trade-off of luminous efficiency in this system due to the intense reabsorption of the blue light by the red and green phosphors, and the color balance is difficult to control. Moreover, the different light output degradation rates often induce the unstable white light.[4] These shortcomings limit the use of LEDs in general lighting applications, therefore, searching for single-component full-color emitting phosphors are necessary for UV-LED chips excitation to improve the luminescence reproducibility and efficiency, which also possess the advantages of low cost and small color aberration.

β-$Ca_3(PO_4)_2$ and its variations are of importance compounds which have been extensively investigated for bioceramics.[5] In recent years, a lot of interests were devoted into the rare earth (RE) ions (Eu^{2+}, Tb^{3+}, Ce^{3+} etc.) and Mn^{2+}doped phosphates luminescence materials, in which the tetrahedral rigid three-dimensional matrix of phosphate is thought to be ideal for charge stabilization.[6] Chen[7] group develop Eu^{2+} doped novel $Sr_8MgLn(PO_4)_7$ (Ln = Y, La, Sc, Gd, Lu) phosphors which can be excited at 250-450 nm and emit broad bands ranging from 450 to 800 nm. Eu^{2+}, Mn^{2+} co-doped $Ca_9Ln(PO_4)_7$ (Ln = La, Y, Gd, Lu) have been considered to be the single-component white emission phosphors for UV LEDs.[8] In 2012, Zhao et al reported

[a]State Key Laboratory of Rare Earth Resource Utilization, Changchun Institute of Applied Chemistry, Chinese Academy of Sciences, Changchun 130022 (P. R., China.). Email: jlin@ciac.ac.cn; hzlian@ciac.ac.cn. Fax: +86-431-85698041; Tel: +86-431-85262031
[b]University of Chinese Academy of Sciences, Beijing 100049 (P. R., China.)

†Electronic supplementary information (ESI) available.

that Ce^{3+} also can sensitize the Mn^{2+} ions in $Ca_9Lu(PO_4)_7$ host,[9] however, the green-component is lacked for single-component white emission. As an efficient green emission activator, Tb^{3+} often has been introduced into some hosts based on its $^5D_4 \rightarrow {}^7F_j$ transition, and it also can be sensitized by Ce^{3+} or Eu^{2+} ions to enhance its emission intensity.[10] The compound $Ca_9Bi(PO_4)_7$ with whitlockite structure was firstly reported by Golubev, V. and Lazoryak, B. in 1991, which is similar to β-$Ca_3(PO_4)_2$ and also isostructural with $Ca_9Fe(PO_4)_7$.[11] Co-doping Eu^{2+} and Dy^{3+} into it produces a new long-lasting phosphorescence phosphor, which has been reported by Jia et al recently.[12] To the best of our knowledge, the photoluminescence properties of Ce^{3+}, Tb^{3+}, Mn^{2+} co-doped $Ca_9Bi(PO_4)_7$ have not been reported. In this article, we developed the Ce^{3+} single doped and Ce^{3+}, Tb^{3+}, Mn^{2+} co-doped $Ca_9Bi(PO_4)_7$ phosphors, which show the tunable emission color including white originating from the energy transfer from Ce^{3+} to Tb^{3+} and Mn^{2+}. The energy transfer mechanisms from Ce^{3+} to Tb^{3+} or Mn^{2+} and the decay times also have been systematically investigated. In addition, the photoluminescence-dependent spectra of the selected sample have been measured, which show its excellent thermal stability of photoluminescence relative to the $Ca_9Gd(PO_4)_7$:Eu^{2+},Mn^{2+}.[7c] These above results suggest their potential application for UV-pumped LEDs.

2. Experiment section

2.1 Materials and preparation

The objective powder samples with the nominal chemical composition $Ca_{9-z}Bi_{1-x-y/l}(PO_4)_7$:$xCe^{3+}$, y/lTb^{3+}, zMn^{2+}[CBPO:xCe^{3+}, yTb^{3+}, zMn^{2+} (x = 0-0.10, y = 0-0.90 , l = 0-0.25, z = 0-0.50 are the mole dopant concentrations)] were prepared via the high-temperature solid-state reaction method under reductive atmosphere. $CaCO_3$ (A.R.), Bi_2O_3 (A.R.), $NH_4H_2PO_4$ (A.R.) and CeO_2 (99.99%), Tb_4O_7 (99.99%), $MnCO_3$ (A.R.) without any purity, were employed as the raw materials. In a typical process, the raw materials were weighed according to the given stoichiometric ratio and mixed thoroughly by grinding them in an agate mortar with appropriate ethanol addition for about 20 min, then the mixtures were sent into the baking box with the temperature of 60 °C to dry them, after which they were shifted to the crucible and transformed to the tube furnace to calcine at 1200 °C for 7 h under 20%H_2/80%N_2 atmosphere condition to generate the final samples followed by regrinding for 1 min. After calcination, the samples were furnace-cooled to room temperature with continual reductive current, and then ground again into powder for the subsequent measurements.

2.2 Characterization

D8 Focus diffractometer was utilized to measure the X-ray diffraction (XRD) patterns at a scanning rate of 10°min^{-1} in the 2θ range from 10° to 110° with graphite-monochromatized Cu K_α radiation (λ = 0.15405 nm). Infrared spectra were collected on a VERTEX 70 Fourier transform infrared (FT-IR) spectrometer (Bruker). The Hitachi F-7000 spectrophotometer equipped with a 150 W xenon lamp as the excitation source was used to conduct photoluminescence (PL) measurements. The luminescence decay lifetimes were measured and obtained from a Lecroy Wave Runner 6100 Digital Osilloscope (1 GHz) using a tunable laser (pulse width = 4 ns, gate = 50 ns) as the excitation (Contimuum Sunlite OPO) source. PL quantum yields (QYs) of phosphors were obtained directly by the absolute PL quantum yield measurement system (C9920−02, Hamamatsu Photonics K. K., Japan). All the above measurements were performed at room temperature (RT). Moreover, the temperature-dependent (25-250 ℃) PL spectra were recorded on a fluorescence spectrophotometer equipped with a 450 W xenon lamp as the excitation source (Edinburgh Instruments FLSP-920) with a temperature controller. Thermogravimetry analysis (TGA) was carried out on a Netzsch STA 409 thermoanalyzer with a heating rate of 10 °C/min in air atmosphere.

3. Results and discussion

3.1. DSC and FT-IR analysis

As depicted in Fig. 1, the DSC-TG curves of CBPO were investigated to analyze pyrolysis behavior and crystallization process, which indicates that the weight loss of precursor takes place constantly from room temperature to 1200 °C in the TG curve. Typically, it is apparent that there are several rough stages in the whole operated temperature range according to TG-DSC curves. Firstly, the water absorbed at the surface of the sample evaporates from room temperature to 45℃. After that, the weight loss from 45 to 210℃ and 210 to 700℃ can be mainly attributed to the decomposition of phosphate which has low decomposition temperature. Then, the weight loss after 700℃ primarily may originate from the decomposition of calcium carbonate. However, we find that the constantly decrease of mass after 700℃ until 1200℃, which may be ascribed to the insufficient calcination time. So, we adopt the calcination temperature at 1200℃ and a relative long time about 7 h to ensure the enough decomposition of calcium carbonate and the crystallization process of CBPO.

The FT-IR spectra were measured to recognize the existence of orthophosphate in our synthesized samples and judge whether the phase changes when doping rare earth ions into the host. We can easily find that the profiles of selected samples are identical with each other, which indicates that the phases of rare earth ions doped samples are consistent with that of CBPO host sample. Generally, the IR absorption band of $(PO_4)^{3-}$ locates at

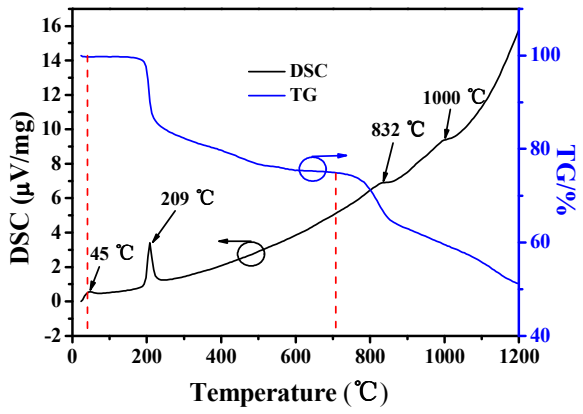

Fig. 1 DSC-TG curves of raw materials from room temperature to 1200°C with a heating rate of 10°C /min in air atmosphere.

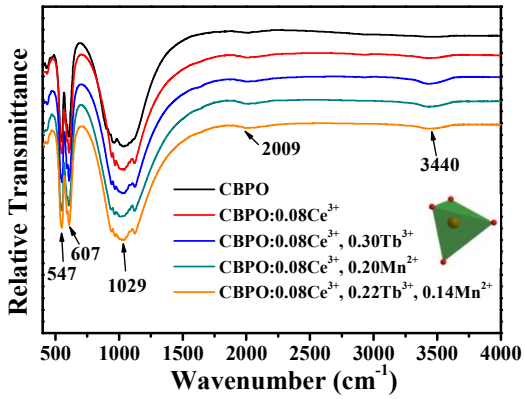

Fig. 2 FT-IR spectra of CBPO host and representative Ce^{3+}, Tb^{3+}, Mn^{2+} doped CBPO samples.

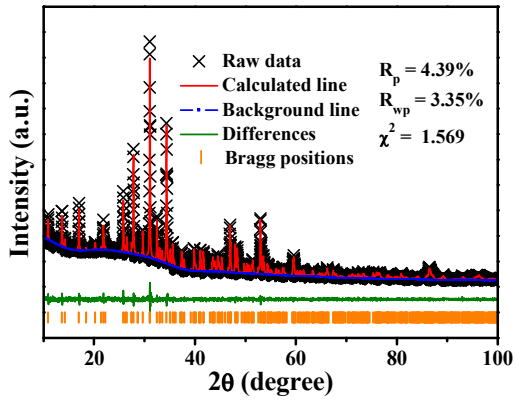

Fig. 3 The Rietveld refinement of powder XRD profile of the representative CBPO:0.08Ce^{3+} sample.

1120-940 cm^{-1} and 650-540 cm^{-1},[13] which include the three absorption peaks observed at 547, 607 and 1029 cm^{-1}, corresponding to the symmetric stretching mode of $(PO_4)^{3-}$ units. Another two peaks at about 2009 and 3440 cm^{-1} are assigned to OH^- vibrations resulting from the covered water on the surface of phosphors under air condition.

3.2 Crystal structure, Phase Identification and Purity.

Fig. 3 shows the Rietveld analysis pattern for XRD data of the representative CBPO:0.08Ce^{3+} sample by using GASA system.[14] The red solid lines and black crosses represent calculated patterns and raw experimental patterns, respectively. The orange short vertical lines point out the position of Bragg reflections of the calculated pattern from the crystal structure of CBPO. The differences between the calculated and experimental results are signed with olive bars which are depicted between the background line (blue line) and the Bragg reflection line. The structure of $Ca_9Fe(PO_4)_7$ (ICSD #82032), which is identical with CBPO, is employed as the initial model for the Rietveld analysis. The refined results indicate that all atom coordinates, fraction factors, as well as thermal vibration parameters were fitted well the reflection condition, R_p = 4.39%, R_{wp} = 3.35% and χ^2 = 1.569, which illustrates there is no detectable impurity phase observed in this obtained sample. The final parameters of crystallography and refined data are listed in Table 1. These results show that the sample is well crystallized in rhombohedral with the space group *R3c*(161). Fig. 4 illustrates the representative XRD patterns of CBPO host and Ce^{3+}, Tb^{3+}, Mn^{2+} doped CBPO samples, as well as the standard pattern of CBPO. It is apparent that all the diffraction peaks are well assigned to the pure phase of CBPO (JCPDS 46-0408) without any impurity, indicating that the as-prepared samples are single phase, and the incorporations of Ce^{3+}, Tb^{3+} and Mn^{2+} don't result in any significant change in the host structure. Fig. 5 presents the details of crystal structure of CBPO (red, white, black and orange balls represent oxygen, calcium, bismuth and phosphorus atoms, respectively), from which we can observe that there are only one kind of Bi^{3+} and three kinds of Ca^{2+} ionic sites, and they are coordinated with six, seven, seven, six oxygen atoms, respectively. The Ce^{3+} and Tb^{3+} ions are expected to substitute Ca^{2+} or Bi^{3+} lattice positions based on their ionic radii [r(Ce^{3+}) = 1.01 Å, r(Tb^{3+}) = 0.92 Å and r(Ca^{2+}) = 1.00 Å, r(Bi^{3+}) = 0.99 Å for coordination number (CN) = 6; r(Ce^{3+}) = 1.07 Å, r(Tb^{3+}) = 1.02 Å and r(Bi^{3+}) = 1.07 Å, r(Ca^{2+}) = 1.07 Å for CN = 7], respectively. Mn^{2+} ions intend to replace Ca^{2+} ions for the reason of their same valance and close ionic radii.

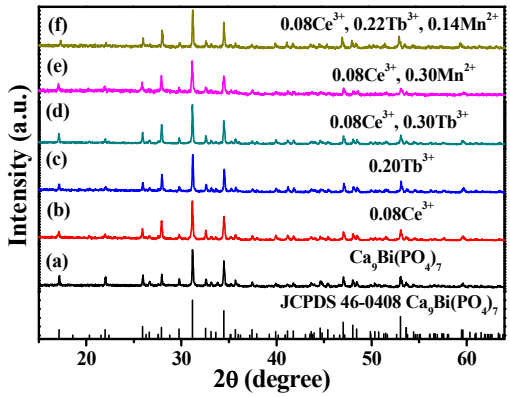

Fig. 4 The powder XRD patterns of the representative CBPO host (a), CBPO:0.08Ce^{3+} (b), CBPO:0.20Tb^{3+} (c), CBPO:0.08Ce^{3+}, 0.30Tb^{3+} (d), CBPO:0.08Ce^{3+}, 0.30Mn^{2+} (e), CBPO:0.08Ce^{3+}, 0.22Tb^{3+}, 0.14Mn^{2+} (f), as well as the standard reference of $Ca_9Bi(PO_4)_7$ JCPDS (46-0408).

Table 1 Crystallographic data and details in the data collection and refinement parameters for the CBPO:0.08Ce^{3+} phosphor

Formula	CBPO:0.08Ce^{3+}
Space group	*R3c*(161)
Symmetry	rhombohedral
a, Å	10.4422(1)
b, Å	10.4422(1)
c, Å	37.3977(4)
V, $Å^3$	3531.50(6)
Z	6
2θ-interval, °	10-100
R_p	4.39
R_{wp}	3.35
χ^2	1.569

3.3 Photoluminescence and energy transfer properties

Fig. 6 shows the PL emission and excitation spectra of CBPO:0.08Ce^{3+} phosphor. The excitation spectrum monitored

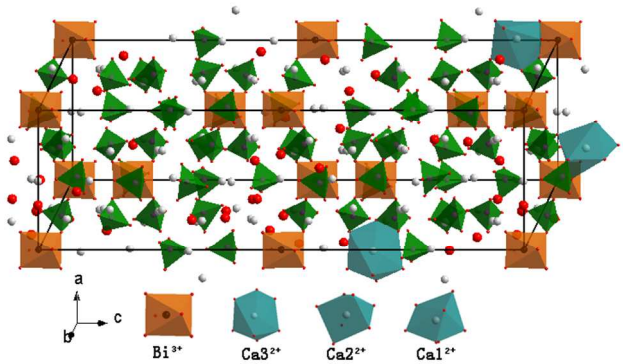

Fig. 5 Crystal structure of $Ca_9Bi(PO_4)_7$ and coordination environments of different Bi^{3+} and Ca^{2+} ions.

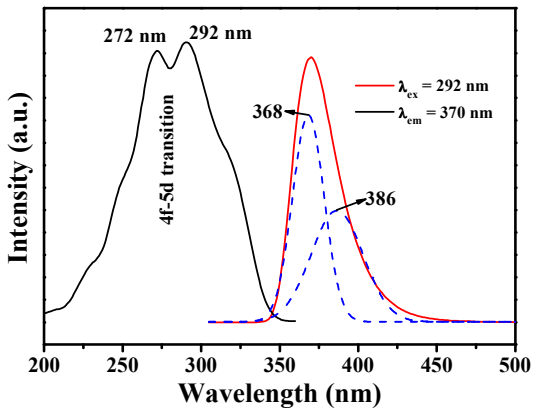

Fig. 6 PL emission and excitation spectra of as-prepared CBPO:0.08Ce^{3+} sample.

at 370 nm of the sample displays a broad band ranging from 200 to 350 nm with two clear peaks at 272 and 292 nm, which are derived from the 4f-5d transition of Ce^{3+}. Upon 292 nm UV excitation, the emission spectrum of as-prepared sample presents an asymmetric broad band extending from 340 to 470 nm with the maximum at about 370 nm, which is ascribed to the Ce^{3+} $5d^1 \rightarrow 4f^1$ allowed transition. As we know, the spin-orbit interaction will arouse the splitting of the energy level 5d of Ce^{3+}, which results in the two ground states ($^2F_{5/2}$ and $^2F_{7/2}$) with an energy difference of about 2000 cm^{-1}.[15] As described above, there is only one kind of Bi^{3+} site in the structure for Ce^{3+} occupation, herein, the emission spectrum can be decomposed into two symmetric broad bands peaking at 368 and 386 nm using Gaussian fitting. However, the energy difference between 368 and 386 nm is about 1267 cm^{-1}, which is far from 2000 cm^{-1}. Therefore, we propose that Ce^{3+} can also occupy Ca^{2+} sites beside Bi^{3+} sites based on their similar ionic radii, which agrees with that mentioned above. The emission spectra of a series of different Ce^{3+} doped CBPO samples and their emission intensities are presented in Fig. 7a and b, respectively. With increasing Ce^{3+} concentration, the profile and emission peak position hardly change while the emission intensity at 370 nm increases until x = 0.08, beyond which the Ce^{3+} emission intensity begins to decrease owing to the general concentration quenching effect. Therefore, we choose the optimal Ce^{3+} concentration x = 0.08 to sensitize Tb^{3+} and Mn^{2+} in subsequent co-doped samples.

As a green emitting activator, Tb^{3+} can be incorporated into many hosts as the efficient green emission component via the energy

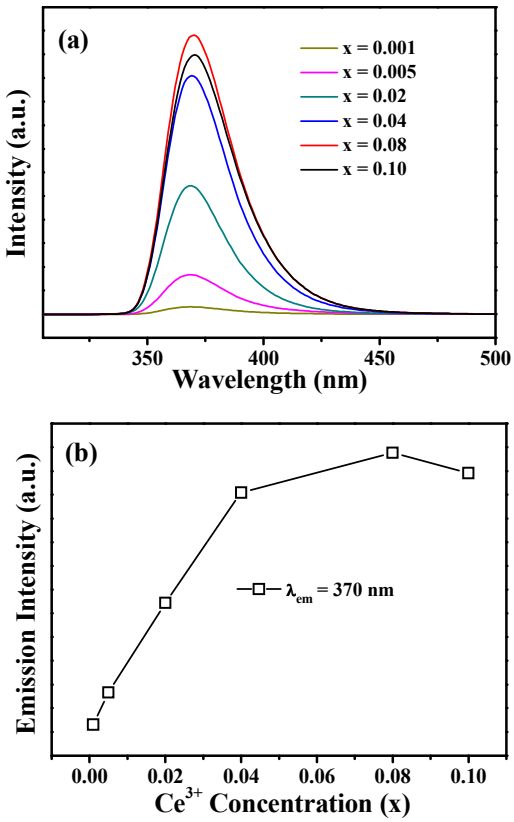

Fig. 7 (a) PL emission spectra of as-prepared CBPO:xCe^{3+} samples. (b) Dependence of emission intensity on Ce^{3+} concentration.

transfer from the sensitizer to it.[16] In this host, we first introduce Tb^{3+} into it to study its characteristic PL property. As depicted in Fig. 8a, the excitation spectrum monitored at 548 nm of CBPO:0.20Tb^{3+} sample primarily contains a broad band centered at 226 nm, which is attributed to the spin-allowed transition from the 4f to the 5d state of Tb^{3+}, and other many lines correspond to the absorption of the spin-forbidden 4f-4f transition. Upon 226 nm excitation, the emission spectra of as-prepared samples consist of both the $^5D_3 \rightarrow {}^7F_J$(J=6,5,4,3,2) and $^5D_4 \rightarrow {}^7F_J$(J=6,5,4,3) transitions of Tb^{3+} ions. The energy gap between $^5D_3$ and $^5D_4$ is close to that between $^7F_0$ and $^7F_6$, which often corresponds to the energy transfer of identical centers:$^5D_3$ (Tb^{3+}) + $^7F_6$ (Tb^{3+}) → $^5D_4$ (Tb^{3+}) + $^7F_0$ (Tb^{3+}).[17] Therefore, the emission spectra between $^5D_3$ and $^5D_4$ change with the increase of Tb^{3+} concentration. In the emission spectra for low Tb^{3+} doping concentrations (l≤0.04), the $^5D_3 \rightarrow {}^7F_J$(J=6,5,4,3,2) transitions predominates them, while the $^5D_3 \rightarrow {}^7F_J$(J=6,5,4,3,2) transitions are predominant when the l > 0.04. As depicted in Fig. 8b, with increasing Tb^{3+} concentration, the emission intensity of $^5D_3$ and $^5D_4$ both increases within Tb^{3+} concentration l = 0.04 upon 226 nm excitation. The $^5D_3$ emission intensity begins to decrease with further Tb^{3+} concentration, while the emission intensity of $^5D_4$ still increase until l = 0.20 , which is originated from the cross relaxation between the $^5D_3$-$^5D_4$ and $^7F_0$-$^7F_6$ of the two neighboring Tb^{3+}, as presented above. The final drop of $^5D_4$ emission intensity owes to the general concentration quenching effect. The concentration quenching of luminescence is derived from the energy migration among the activators at high concentrations. In the process of energy migration, the excitation energy will

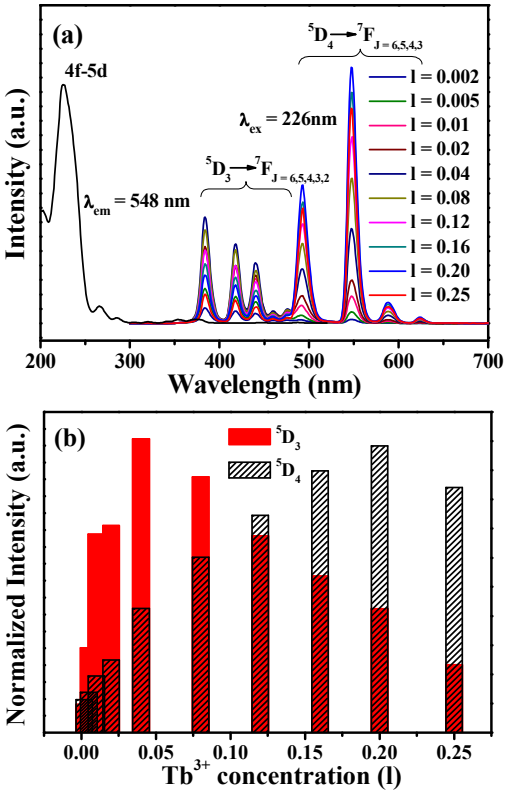

Fig. 8 (a) PL emission spectra of as-prepared CBPO:lTb^{3+} samples. (b) Dependence of $^5D_3$ and $^5D_4$ emission intensities on Tb^{3+} concentration.

be lost at a killer or quenching site, leading to the drop of PL intensity.

Fig. 9a and b show the PL excitation and emission spectra as well as the emission intensity of Ce^{3+} and Tb^{3+} as a function of Tb^{3+} concentration. As depicted in Fig. 9a, the excitation spectra monitored at 370 (Ce^{3+} emission) and 548 nm (Tb^{3+} emission) show the similar profiles with the excitation extent from 250 to 350 nm, while the latter one owns its characteristic excitation extent from 200 to 250 nm originating from Tb^{3+} 4f-5d transition, which occurs in Tb^{3+} single doped samples above. This gives the confirmation that most of energy of Tb^{3+} emission excited at 292 nm derives from Ce^{3+} when Ce^{3+} and Tb^{3+} are co-doped into the CBPO host. Seen from the emission spectra, Ce^{3+} emission intensities decrease monotonously with the increase of Tb^{3+} concentration which is contrary to that of Tb^{3+} emission, as shown in Fig. 9b. There is no saturation of Tb^{3+} emission intensity which is often originated from concentration though y has been adopted as 0.9. This illustrates that Tb^{3+} can be well incorporated into this host, and some Tb^{3+} may occupy Ca^{2+} sites, as supposed above. The decay curves were plotted in Fig. 9c to show the decay properties of samples. As they deviate from exponential functions, the average lifetime τ can be defined as:[18]

$$\tau = \frac{\int_0^\infty tI(t)dt}{\int_0^\infty I(t)dt} \quad (1)$$

where $I(t)$ is the luminous intensity at time t. According to the equation, the luminescence lifetimes of Ce^{3+} are determined to be 36.0, 28.7, 26.6, 22.1 and 17.9 ns for Tb^{3+} concentrations of 0, 0.14, 0.30, 0.60 and 0.90, respectively. The monotonous drop

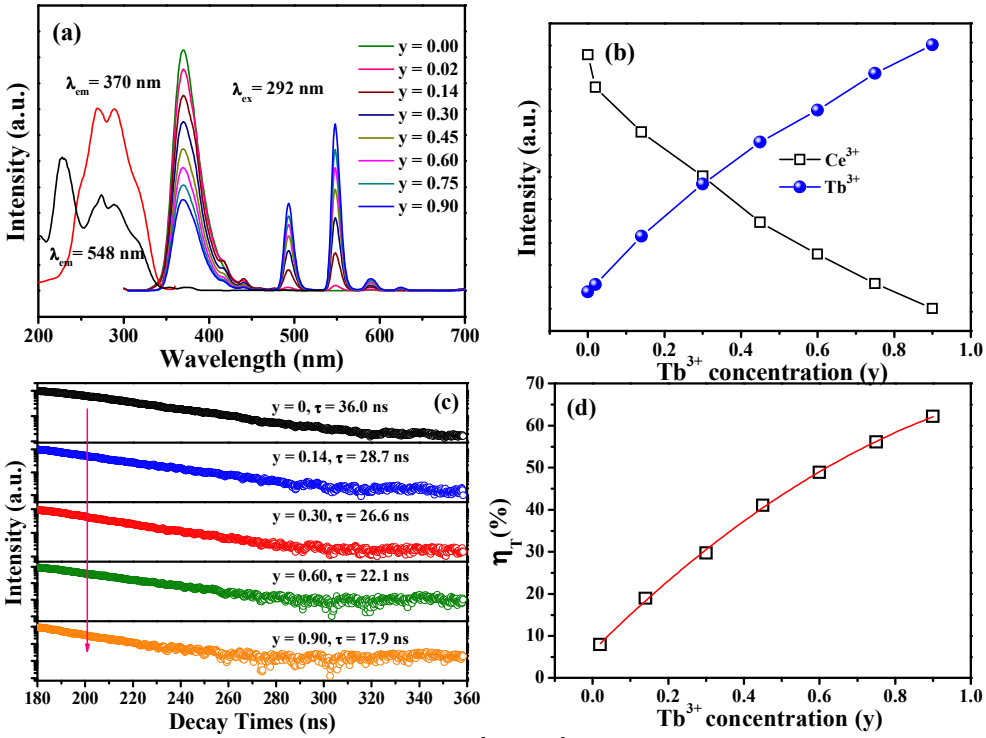

Fig. 9 (a) PL emission spectra of as-prepared CBPO:0.08Ce^{3+}, yTb^{3+} samples and excitation spectrum of CBPO:0.08Ce^{3+}, 0.90Tb^{3+}. (b) Dependence of emission intensities of Ce^{3+} and Tb^{3+} on Tb^{3+} concentration excited at 292 nm. (c) Variation of decay curves of Ce^{3+} emission with different Tb^{3+} concentration. (d) Dependence of energy efficiency, η_T on Tb^{3+} doping concentration (y).

in the lifetimes of Ce^{3+} with increasing Tb^{3+} concentration y, further certifies an energy transfer from Ce^{3+} to Tb^{3+} ions. The energy transfer efficiency (η) from Ce^{3+} to Tb^{3+} in CBPO:0.08Ce^{3+}, yTb^{3+} can be approximately calculated using the following expression:[19]

$$\eta_T = 1 - \frac{I_S}{I_{S0}} \quad (2)$$

where η_T is the energy transfer efficiency and I_{S0} and I_S are the luminescence intensity of Ce^{3+} ions without and with of Tb^{3+} ions, respectively. The energy transfer efficiency monotonously ascends with continuous increase in Tb^{3+} concentration while the increasing rate decreases because of the restriction of the energy transfer from Ce^{3+} to Tb^{3+} ions with fixed Ce^{3+} concentration. The maximum value can reach about 62% in our operated range.

Similarly, the constant decrease of emission intensity of Ce^{3+} excited at 292 nm can be clearly found in Fig. 10a and b, however, the Mn^{2+} emission intensity increases to maximum at z = 0.4, beyond which its emission intensity will falls because of the concentration quenching effect, as depicted in Fig. 10b, which illustrate the energy transfer from Ce^{3+} to Mn^{2+} ions. The luminescence lifetimes supplied decrease from 36 to 19.2 ns corresponding to Mn^{2+} concentration z = 0 to 0.50 in Fig. 10c, which also give a confirmation to the energy transfer from Ce^{3+} to Mn^{2+} ions in Ce^{3+}, Mn^{2+} co-doped CBPO phosphors. The energy transfer efficiency can reach about 79%, as plotted in Fig. 10d, according to the above formula (2).

In order to determine the energy transfer mechanism in CBPO:0.08Ce^{3+},yTb^{3+}/zMn^{2+} samples, it is necessary to know the critical distance (R_c) between activators (Ce^{3+}) and acceptors (Tb^{3+}/Mn^{2+}) here. With the increase of Tb^{3+}/Mn^{2+} content, the distance between Ce^{3+} and Tb^{3+}/Mn^{2+} ions becomes shorter and shorter, thus the probability of energy migration increases. When the distance reaches small enough, the concentration quenching occurs and the energy migration is hindered. Therefore, the calculation of R_c has been pointed out by Blasse:[20]

$$R_c \approx 2\left[\frac{3V}{4\pi X_c N}\right]^{1/3} \quad (3)$$

where V refers to the volume of the unit cell, N is the number of host cations in the unit cell, and X_c is defined as the critical concentration of dopant ions (total concentration of Ce^{3+} and Tb^{3+}/Mn^{2+}, approximately 0.70/0.37), that is, at which the luminescence intensity of Ce^{3+} is half of that in the sample without Tb^{3+}/Mn^{2+}. For the CBPO host, N = 6, V = 3551.66 Å^3, and X_c is about 70/37% here; Accordingly, the critical distance (R_c) was estimated to be about 11.73/23.03 Å.

In general, exchange interaction, radiation reabsorption, and electric multipolar interaction are considered as the three mechanisms for non-radiate energy transfer. The result calculated above indicates the little possibility of exchange interaction since the exchange interaction is predominant only for about 5 Å.[21] The mechanism of radiation reabsorption is only efficacious when the fluorescence and absorption spectra are widely overlapping, which is

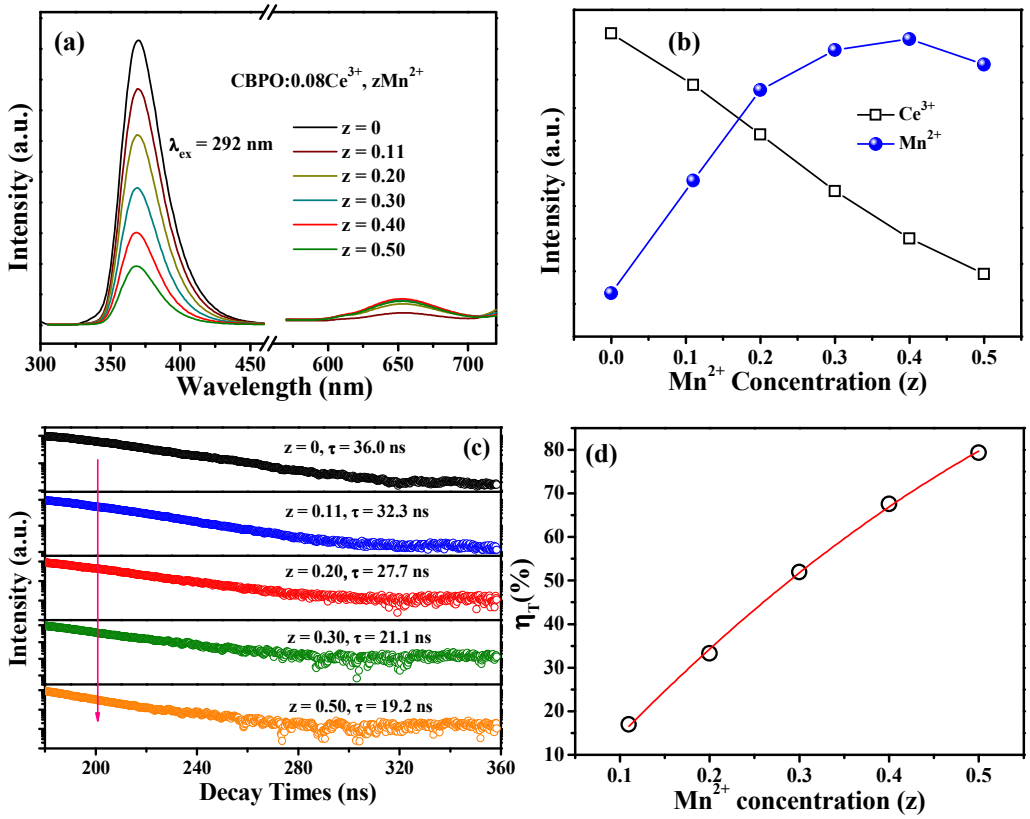

Fig. 10 (a) PL emission spectra of as-prepared CBPO:0.08Ce^{3+}, zMn^{2+} samples excited at 292 nm. (b) Dependence of emission intensities of Ce^{3+} and Mn^{2+} on Mn^{2+} concentration excited at 292 nm. (c) Variation of decay curves of Ce^{3+} emission with different Mn^{2+} concentration. (d) Dependence of energy efficiency, η_T on Mn^{2+} doping concentration (y).

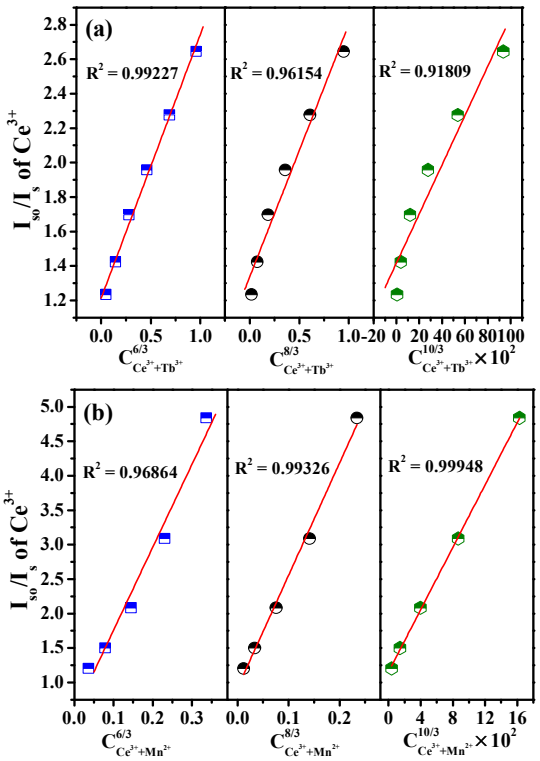

Fig. 11 (a) I_{S0}/I_S - $C^{\alpha/3}$ plots of Ce^{3+}, Tb^{3+} co-doped CBPO phosphors. (b) I_{S0}/I_S - $C^{\alpha/3}$ plots of Ce^{3+}, Mn^{2+} co-doped CBPO phosphors.

not likely to occur in this case. As a consequence, we can infer the energy transfer mechanism from Ce^{3+} to Tb^{3+}/Mn^{2+} ions is likely to be electric multipolar interactions. According to the Dexter's energy transfer formula of multipolar interaction and Reisfeld's approximation, the following relationship can be used:[22]

$$\frac{\eta_{S0}}{\eta_S} \propto C^{\alpha/3} \quad (4)$$

where η_{S0} and η_S represent the luminescence quantum efficiencies of the Ce^{3+} ions with the absence and presence of the Tb^{3+}/Mn^{2+} ions, respectively. C is the total concentration of the Ce^{3+} and Tb^{3+}/Mn^{2+} ions. The value for α = 6, 8, and 10 corresponds to dipole-dipole, dipole-quadrupole, and quadrupole-quadrupole interactions, respectively. However, the value of η_{S0}/η_S is difficult to be acquired and therefore it can be assessed instead by the I_{S0}/I_S, where I_{S0} and I_S refer to the luminescence intensity of the Ce^{3+} ions without and with the Tb^{3+}/Mn^{2+} ions, respectively, the following relationship can be obtained:[23]

$$\frac{I_{S0}}{I_S} \propto C^{\alpha/3} \quad (5)$$

The relationship between I_{S0}/I_S and $C^{\alpha/3}$ based on the above equation are illustrated in Fig. 11. The results show that the I_{S0}/I_S - $C^{6/3}$ plot can be fitted linearly better than the other two plots for Ce^{3+}, Tb^{3+} co-doped samples, while it is I_{S0}/I_S - $C^{10/3}$ plot for Ce^{3+}, Mn^{2+} co-doped samples in Fig. 11a and b, respectively. Therefore, they demonstrate the energy transfer from Ce^{3+} to Tb^{3+} and Mn^{2+} ions takes place through the dipole-dipole and quadrupole-quadrupole interaction mechanisms, respectively, which is coincided with the relationship between τ_{S0}/τ_S and $C^{\alpha/3}$ in the Fig. S1 (see ESI†).

3.4 CIE chromaticity coordinates, quantum yields and thermal properties

A series of Ce^{3+}, Tb^{3+} and Mn^{2+} co-doped CBPO samples have been prepared to tune the emission colors, which can change from purple-blue to green and final red by adjusting the concentration ratio between Tb^{3+}/Mn^{2+} ions with stationed Ce^{3+} concentration. The corresponding luminescence photos of various samples under 302 nm UV lamp radiation are shown in Fig. 12 (left). The corresponding CIE chromaticity coordinates and quantum yields of some representative samples are listed in Table 2, which show the CIE chromaticity coordinate shifts from 1(0.166, 0.011) to 3(0.260, 0.569) with increasing Tb^{3+} concentration from y = 0 to 0.90 in CBPO:0.08Ce^{3+}, yTb^{3+} samples, and from 1(0.166, 0.094) to 6(0.582, 0.287) corresponding to Mn^{2+} concentration z =0 to 0.50 in CBPO:0.08Ce^{3+}, zMn^{2+} samples upon 292 nm excitation. After making an effort, a warm white light has been realized in CBPO:0.08Ce^{3+}, 0.22Tb^{3+}, 0.11Mn^{2+} with the absolute quantum yield of 50% and CIE chromaticity coordinate of (0.375, 0.310) upon 292 nm excitation, as signed in Fig 12 (right). Additionally, the maximum absolute quantum yield is 84% for CBPO:0.08Ce^{3+}, 0.90Tb^{3+} sample, and it can be improved by the optimization of experimental condition, grain size and morphology.

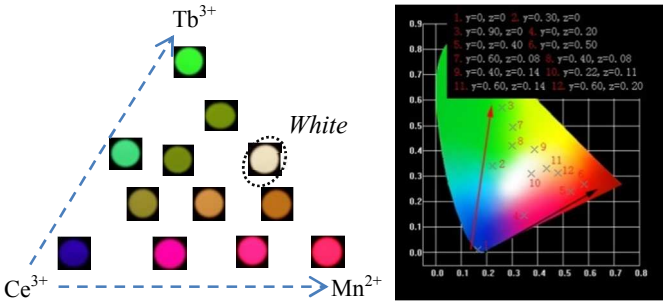

Fig. 12 Variation of emission color with different concentrations of Tb^{3+} and Mn^{2+} in CBPO:0.08Ce^{3+}, yTb^{3+}, zMn^{2+} under 302 nm UV lamp excitation on the left and of CIE chromaticity coordinates corresponding to the representative samples upon 292 nm excitation on the right.

Thermal stability is one of the most important parameters that should be taken into account for the fabrication of LEDs. In general, the phosphors should keep their emission intensity at high temperature above 150 °C because quantity of heat has been constantly produced in the LEDs after operating a period of time. To investigate the influence of temperature on luminescence, the temperature-dependent PL emission spectra (298 K-523 K) for white-emitting phosphor CBPO:0.08Ce^{3+}, 0.22Tb^{3+}, 0.11Mn^{2+} under 292 nm excitation are plotted in Fig. 13a. The results display a continual decrease in emission intensity with increasing temperature from 25 to 250 °C due to thermal quenching via phonon interaction, in which the excited luminescence center is thermally activated through the crossing point between the ground and the excited states.[24] In addition, the emission peaks of Ce^{3+} and Tb^{3+} keep nearly unchanged, as well as for Mn^{2+} emission band with the increasing temperature, which is similar to the result discussed.[25] The activation energy (E_a) for thermal quenching phenomenon can be acquired by the following formula proposed by Arrhenius:[26]

$$In\left(\frac{I_0}{I}\right) = InA - \frac{E_a}{kT} \quad (6)$$

Table 2 CIE chromaticity coordinates and quantum yields of CBPO:0.08Ce^{3+}, yTb^{3+}, zMn^{2+} upon 292 nm excitation

Sample	CIE coordinates (x, y)	QY(%)
y = 0	(0.166, 0.011)	52
y = 0.14, z = 0	(0.205, 0.201)	55
y = 0.30, z = 0	(0.223, 0.341)	61
y = 0.45, z = 0	(0.240, 0.395)	65
y = 0.60, z = 0	(0.248, 0.457)	73
y = 0.75, z = 0	(0.255, 0.507)	77
y = 0.90, z = 0	(0.260, 0.569)	84
y = 0, z = 0.11	(0.288, 0.096)	47
y = 0, z = 0.20	(0.347, 0.175)	38
y = 0, z = 0.30	(0.438, 0.219)	31
y = 0, z = 0.40	(0.529, 0.260)	28
y = 0, z = 0.50	(0.582, 0.287)	24
y = 0.40, z = 0.08	(0.299, 0.421)	52
y = 0.60, z = 0.08	(0.302, 0.493)	60
y = 0.22, z = 0.11	(0.375, 0.310)	50
y = 0.40, z = 0.14	(0.387, 0.404)	36
y = 0.60, z = 0.14	(0.436, 0.330)	44
y = 0.60, z = 0.20	(0.479, 0.312)	37

where I_0 and I are the original PL intensity of the phosphor at room temperature and given temperature, respectively. k refers to Boltzmann constant (8.626×10^{-5} eV), A is a constant, and E_a is the activation energy for thermal quenching. The relationship of $\ln(I_0/I-1)$ versus 1/kT of the Ce^{3+}, Tb^{3+} and Mn^{2+} co-doped phosphors CBPO:0.08Ce^{3+}, 0.22Tb^{3+}, 0.11Mn^{2+} is illustrated in Fig. 13b. The value of E_a is determined to be 0.1949 eV according to the slope of the fitting line. The activation energy is lower with respect to Sr_2SiO_4:Eu^{2+} (0.22 eV), $SrSiO_2N_2$:Eu^{2+} (0.24 eV), $(Sr,Ba)_2SiO_4$:Eu^{2+} (0.2678 eV) phosphors.[27,7b]

4. Conclusions

In summary, single-composition and color-tunable Ce^{3+}, Tb^{3+} and Mn^{2+} doped CBPO phosphors have been prepared via the high-temperature solid-state reaction process. In addition, their luminescence properties and energy transfer behavior have been investigated. The energy transfer from Ce^{3+} to Tb^{3+}/Mn^{2+} has been demonstrated to be the dipole-dipole/quadrupole-quadrupole interaction mechanism, respectively. Therefore, the emission color can be tuned from purple-blue to green/red with increasing Tb^{3+}/Mn^{2+} concentration at the certain Ce^{3+} content in CBPO:Ce^{3+}, Tb^{3+}/Mn^{2+} phosphors. Based on the energy transfer effect, single-component white-light-emitting CBPO:0.22Ce^{3+}, 0.22Tb^{3+}, 0.11Mn^{2+} phosphor has been realized with the absolute quantum yield of 50% and CIE chromaticity coordinate of (0.375, 0.310) upon 292 nm excitation. More noticeable is its good thermal property, which shows about 83.6% at 150 °C of its initial PL intensity at room temperature. The present results show that the as-prepared phosphor show potential to be a single-component white-light phosphor for application in UV w-LED devices.

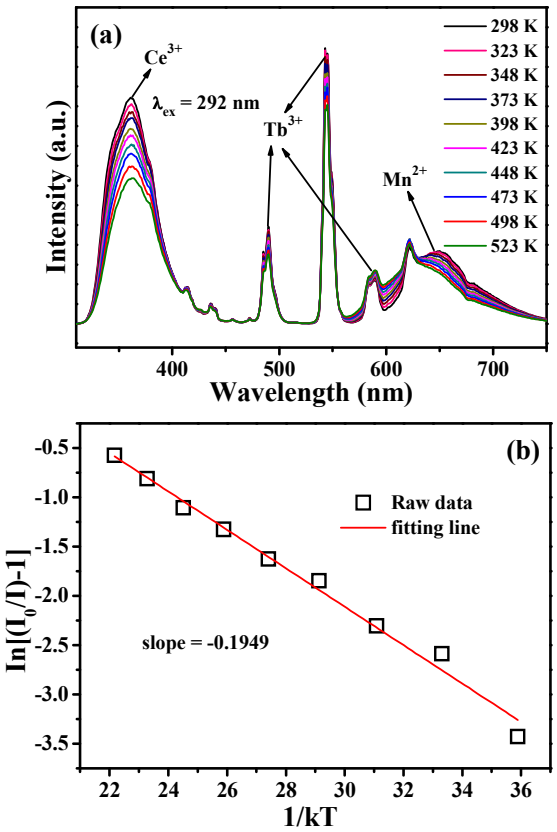

Fig. 13 (a) Temperature-dependent PL spectra of CBPO:0.08Ce^{3+}, 0.22Tb^{3+}, 0.11Mn^{2+} phosphor (λ_{ex} = 292 nm). (b) The relationship of $\ln(I_0/I-1)$ versus 1/kT activation energy graph for thermal quenching of CBPO:0.08Ce^{3+}, 0.22Tb^{3+}, 0.11Mn^{2+} sample.

Acknowledgments

This project is financially supported by the National Natural Science Foundation of China (NSFC Grants 51472234, 51172227, 91433110), National Basic Research Program of China (Grants 2014CB643803), and Joint Funds of the National Natural Science Foundation of China (Grant U13012038).

References

1 (a) S. Gandhi, K. Thandavan, B. J. Kwon, H. J. Woo, K. Jang and D. S. Shin, *Ceram. Inter.*, 2014, **40**, 5245; (b) D. Geng, H. Lian, M. Shang, Y. Zhang and J. Lin, *Inorg. Chem.*, 2014, **53**, 2230; (c) J. Zhou and Z. Xia, *J. Lumin.*, 2014, **146**, 22; (d) X. Zhao, L. Fan, T. Yu, Z. Li and Z. Zou, *Opt. Express*, 2013, **21**(25), 31660; (e) H. Liu, Y. Luo, Z. Mao, L. Liao and Z. Xia, *J. Mater. Chem. C*, 2014, **2**, 1619; (f) H. Zhu, C. C. Lin, W. Luo, S. Shu, Z. Liu, Y. Liu, J. Kong, E. Ma, Y. Cao, R.-S. Liu and X. Chen, *Nature Commun.*, 2014, **5**, 4312.

2 (a) K. H. Lee, S. Choi, H. K. Jung and W. B. Im, *Acta Materialia*, 2012, **60**, 5783; (b) W. Lü, Z. Hao, X. Zhang, Y. Luo, X. Wang and J. Zhang, *Inorg. Chem.*, 2011, **50**, 7846; (c) C. H. Huang, D. Y. Wang, Y. C. Chiu, Y. T. Yeh and T. M. Chen, *RSC Adv.*, 2012, **2**, 9130; (d) W. R. Liu, C. H. Huang, C. W. Yeh, J. C. Tsai, Y. C. Chiu, Y. T. Yeh and R. S. Liu, *Inorg. Chem.*, 2012, **51**, 9636.

3 (a) J. Y. Han, W. B. Im, G. Lee and D. Y. Jeon, *J. Mater. Chem.*, 2012, **22**, 8793; (b) H. Yu, D. Deng, D. Zhou, W. Yuan, Q. Zhao, Y. Hua, S. Zhao, L. Huang and S. Xu, *J. Mater. Chem. C*, 2013, **1**, 5577; (c) J. Sun, D. Cui and H. Du, *Appl. Phys. B*, 2013, **111**, 537; (d) Z. Xia, R. S. Liu, K. W. Huang and V. Drozd, *J. Mater. Chem*., 2012, **22**, 15183.
4 (a) Z. Wang, P. Li, Z. Yang, Q. Guo and G. Dong, *Ceram. Inter*., 2014, **40**, 15283; (b) M. Zhang, Y. Liang, W. Huang, Z. Xia, D. Yu, Y. Lan, G. Li and W. Zhou, *Mater. Res. Bull*., 2014, **57**, 231.
5 (a) A. C. Tas , S. B. Bhaduri and S. Jalota, *Mater. Sci. & Eng.* C, 2007, **27**,394; (b) K. Lin, J. Chang, J. Lu, W. Wu and Y. Zeng, *Ceram. Inter*., 2007, **33**, 979; (c) S. Ni, K. Lin, J. Chang and L. Chou, *J. Biomed. Mater. Res. A*, 2008, **85**, 72.
6 (a) N. Guo, H. You, C. Jia, R. Ouyang and D. Wu, *Dalton Trans*., 2014, **43**, 12373; (b) C. Zhao, Z. Xia and S. Yu, *J. Mater. Chem. C*, 2014, **2**, 6032; (c) Z. Wang, X. Teng and P. Li, *J. Alloys Compd*., 2014, **589**, 549; (d) T. Jiang, X. Yu, X. Xu, H. Yu, D. Zhou and J. Qiu, *Mater. Res. Bull*., 2014, **51**, 80.
7 (a) C.-H. Huang and T.-M. Chen, *Inorg. Chem*., 2011, **50**, 5725; (b) C.-H. Huang, Y.-C. Chen, T.-M. Chen, T.-S. Chan and H.-S. Sheu, *J. Mater. Chem*., 2011, **21**, 5645; (c) C.-H. Huang, Y.-C. Chiu, Y.-T. Yeh and T.-M. Chen, *Mater. Express*, 2012, **2**, 303; (d) C.-H. Huang, D.-Y. Wang, Y.-C. Chiu, Y.-T. Yeh and T.-M. Chen, *RSC Adv*., 2012, **2**, 9130.
8 (a) C.-H. Huang, P.-J. Wu, J.-F. Lee and T.-M. Chen, *J. Mater. Chem*., 2011, **21**, 10489; (b) C.-H.Huang and T.-M. Chen, *Opt. Express*, 2010, **18**, 5089; (c) N. Guo, H. You, Y. Song, M. Yang, K. Liu, Y. Zheng, Y. Huang and H. Zhang, *J. Mater. Chem*., 2010, **20**, 9061; (d) N. Guo, Y. Huang, H. You, M. Yang, Y. Song, K. Liu and Y. Zheng, *Inorg. Chem*., 2010, **49**, 10907.
9 (a) C. Zhao, X. Yi, Y. Wang, F. Huang and Y. Hang, *J. Lumin*., 2012, **132**, 617.
10 (a) J. Zhang, Y. He, Z. Qiu, W. Zhang, W. Zhou, L. Yu and S. Lian, *Dalton Trans.*, 2014, **43**, 18134; (b) K. Li, J. Fan, X. Mi, Y. Zhang, H. Lian, M. Shang and J. Lin, *Inorg. Chem*., 2014, **53**, 12141.
11 V. Golubev and B. Lazoryak, *Izv. Akad. Nauk SSSR, Neorg.Mater*., 1991, **27**, 376.
12 Y. Jia, H. Li, R. Zhao, W. Sun, Q. Su, R. Pang and C. Li, *Opt. Mater*., 2014, **36**, 1811.
13 G. R. Dillip and B. D. P. Raju, *J. Alloys Compd*., 2012, **540**, 67.
14 C. Larson and R. B. Von Dreele, Generalized Structure Analysis System (GSAS), Los Alamos National Laboratory Report LAUR 86-748, Los Alamos National Laboratory, Los Alamos, NM, 1994.
15 (a) Y. Zhang, D. Geng, M. Shang, Y. Wu, X. Li, H. Lian, Z. Cheng and J. Lin, *Eur. J. Inorg. Chem.,* 2013, **25**, 4389; (b) R. Yu, H. Li, H. Ma, C. Wang and H. Wang, *J. Am. Ceram. Soc*., 2014, **97**, 1.
16 (a) S. Lee and S. Park, *J. Lumin*., 2013, **143**, 215; (b) Z. Xia and R.-S. Liu, *J. Phys. Chem. C*, 2012, **116**, 15604.
17 K.-S. Sohn and N. Shin, *Electrochem. Solid-State Lett*., 2002, **5**, H21.
18 C.-H. Huang, W.-R. Liu, T.-S. Chan and Y.-T. Lai, *Dalton Trans.*, 2014, **43**, 7917.
19 J. Chen, Y. Liu, M. Fang and Z. Huang, *Inorg. Chem*., 2014, **53**, 11396.
20 (a) S. J. Gwak, P. Arunkumar and W. B. Im, *J. Phys. Chem. C*, 2014, **118**, 2686; (b) D. L. Dexter, *J. Chem. Phys*., 1953, **21**, 836.
21 D. L. Dexter, *J. Chem. Phys*., 1969, **21**, 131.
22 (a) D. L. Dexter and J. H. Schulman, *J. Chem. Phys*., 1954, **22**, 1063; (b) C. H. Huang, T. W. Kuo and T. M. Chen, *ACS Appl. Mater. Inter*., 2010, **2**, 1395.
23 (a) K. H. Kwon, W. B. Im, H. S. Jang, H. S. Yoo and D. Y. Jeon, *Inorg. Chem*., 2009, **48**, 11525; (b) Z. Lian, J. Sun, L. Zhang, D. Shen, G. Shen, X. Wang and Q. Yan, *RSC Adv.*, 2013, **3**, 16534; (c) P. Paulose, G. Jose, V. Thomas, N. Unnikrishnan and M. Warrier, *J. Phys. Chem. Solids*, 2003, **64**, 841.
24 Z. G. Xia, X. M. Wang, Y. X. Wang, L. B. Liao and X. P. Jing, *Inorg. Chem*., 2011, **50**, 10134.
25 G. Zhu, S. Xin, Y. Wen, Q. Wang, M. Que and Y. Wang, *RSC Adv*., 2013, **3**, 9311.
26 (a) R. J. Xie and N. Hirosaki, *Appl. Phys. Lett*., 2007, **90**, 191101; (b) Y. Chen, B. Liu, C. Shi, G. Ren and G. Zimmerer, *Nucl. Instrum. Methods Phys. Res. Sect. A*, 2005, **537**, 31.
27 G. Anoop, D. W. Lee, D. W. Suh, S. L. Wu, K. M. Ok and J. S. Yoo, *J. Mater. Chem. C*, 2013, **1**, 4705.

Graphic Abstract

A series of $Ca_9Bi(PO_4)_7$:Ce^{3+}, Tb^{3+}, Mn^{2+} phosphors synthesized via the high-temperature solid-state reaction method can emit intense tunable color from purple-blue to red including white under UV excitation, which shows the potential application in UV-pumped white-light-emitting diodes.